PCCP

PAPER

Cite this: *Phys. Chem. Chem. Phys.*, 2018, **20**, 21113

A progressive metal–semiconductor transition in two-faced Janus monolayer transition-metal chalcogenides†

Yan-Dong Guo,[ab] Hong-Bo Zhang,[ab] Hong-Li Zeng,*[bc] Hai-Xia Da,[ab] Xiao-Hong Yan,*[abd] Wen-Yue Liu[a] and Xin-Yi Mou[a]

Received 8th May 2018,
Accepted 20th July 2018

DOI: 10.1039/c8cp02929f

rsc.li/pccp

Breaking the symmetry in the out-of-plane direction in two-dimensional materials to trigger distinctive electronic properties has long been predicted. Inspired by the recent progress in the experimental synthesis of a sandwiched S–Mo–Se structure (Janus SMoSe) at the monolayer limit [Zhang *et al.*, *ACS Nano*, 2017, **11**, 8192–8198], we investigate the transport and electronic structure of two-faced XMoY monolayers (X, Y = O, S, Se and Te) through first-principles calculations. It is found that all the monolayers are semiconductors except OMoTe, which is metallic. Interestingly, the "parents" of OMoTe (MoO_2 and $MoTe_2$) are both semiconductors. Further analysis shows that it is the out-of-plane asymmetry-induced strain that results in the metal–semiconductor transition between Janus OMoTe and its parents. By increasing the ratio of O atoms in one face of $MoTe_2$, a progressive decreasing trend of the bandgap, as well as the transition to metallic, is found. In addition, a transition from the direct band gap semiconductor to the indirect one is also observed in the process. This could be used as an effective way to precisely control electronic structures, *e.g.*, the bandgap. Different from other methods, this method uses the intrinsic features of the material, which can persist without the need of additional equipment. Moreover, such a modulating method is expected to be extended to many other transition-metal chalcogenides, showing great application potential.

Introduction

In recent years, two-dimensional (2D) materials have attracted much attention due to their peculiar properties originating from the reduction of dimensions from the bulk to monolayer.[1–10] In geometry, a 2D structure possesses two faces, which are expected to be utilized to modulate the electronic properties by creating asymmetry between them. However, in graphene-like materials, there is only one layer of atoms and it is impossible to realize such a structure.[11,12] Although some efforts have been made through doping, the low covering ratio, randomness, and instability make them less practical for realistic devices.[13,14]

Different from graphene, monolayer transition-metal dichalcogenides (TMDs) possess three stacked layers of atoms, showing the possibility of fabricating two-faced materials.[6,15–18] The break of symmetry in the out-of-plane direction in 2D TMDs might trigger interesting electronic properties and lead to various applications, *e.g.*, actuators in the 2D limit and an intrinsic electric field perpendicular to the in-plane direction. Actually, such a two-faced structure has long been predicted in theory, but it has rarely been reported.

Recently, through a controlled sulfurization process, Zhang *et al.*[7] successfully synthesized a crystal configuration of a sandwiched S–Mo–Se structure (Janus SMoSe) at the monolayer limit. There are three layers of atoms in it, *i.e.*, sulfur, molybdenum and selenium from top to bottom. Such a two-faced structure possesses an unconventional asymmetry, quite different from former TMD-based heterojunctions.[7,19–21]

As is well known, some other transition-metal chalcogenides, such as transition-metal oxides, can also form a monolayer structure and share a similar geometry with transition-metal dichalcogenides. They can be denoted as MX_2 structures (M, transition metal; X, chalcogen atom), and there are at least 44 different MX_2 compounds that can form stable 2D monolayer structures.[22] Thus, such a huge database and the synthesis of

[a] *College of Electronic and Optical Engineering, Nanjing University of Posts and Telecommunications, Nanjing 210023, China*
[b] *Key Laboratory of Radio Frequency and Micro Nano Electronics of Jiangsu Province, Nanjing 210023, China*
[c] *College of Natural Science, Nanjing University of Posts and Telecommunications, Nanjing 210046, China. E-mail: hlzeng@njupt.edu.cn*
[d] *College of Science, Nanjing University of Aeronautics and Astronautics, Nanjing 210016, China*

† Electronic supplementary information (ESI) available. See DOI: 10.1039/c8cp02929f

Janus SMoSe open new avenues for the synthesis of various two-faced XMY structures. There is a need to explore the electronic and transport properties of monolayer XMY materials, which may be used in nanoelectronic devices. However, there is still a lack of such studies.

In the present work, we focus on the Janus XMoY monolayers (M is fixed to be Mo; X, Y = O, S, Se and Te) and study their electronic transport, based on density functional theory (DFT) combined with nonequilibrium Green's function (NEGF). Interestingly, it is found that all the Janus XMoY monolayers (OMoS, OMoSe, SMoSe, SMoTe and SeMoTe) exhibit semiconductor behavior except OMoTe, which is metallic. From the structural point of view, MoO_2 and $MoTe_2$ can be seen as the "parents" of OMoTe. However, neither of these parents is metallic, and they are both semiconductors.[22] Further analysis shows that it is the out-of-plane asymmetry-induced strain that results in the metal–semiconductor transition between Janus OMoTe and its parents. Moreover, by increasing the ratio of O atoms in one face of $MoTe_2$, a monotonically decreasing trend of the band gap and the transition to metal are found. Our findings suggest a feasible way to precisely modulate the electronic properties of the Janus XMoY monolayer, and it is expected to be extended to other transition-metal chalcogenides, showing great application potential.

Methodology

To investigate the electronic (especially the transport) properties of the XMoY system, DFT calculations combined with NEGF were preformed, through the Atomistix Toolkit package.[23,24] The mesh cutoff energy was set to be 150 Ry, with $2 \times 1 \times 5$ (for bulk calculations) and $2 \times 1 \times 100$ (for transport calculations) k-point meshes in the Monkhorst–Park scheme.[25] The Perdew–Burke–Eenzerhof (PBE) formulation of the generalized gradient approximation (GGA) was used as the exchange–correlation function.[26] The double-zeta polarized basis set was chosen for the local numerical orbitals. To prevent the interactions with adjacent images, supercells with sufficient vacuum space were employed (more than 10 Å). The geometries were fully optimized until the residual force on each atom was smaller than 0.02 eV $Å^{-1}$.

Results and discussion

Among these kinds of transition-metal chalcogenides, we here confine our attention to XMoY configurations in the H structure,[22] where X, Y = O, S, Se and Te, and the middle layer atoms are fixed as Mo. Considering the combination of these elements, there will be in total six configurations, *i.e.*, OMoS, OMoSe, OMoTe, SMoSe, SMoTe and SeMoTe. In previous studies, their parent configurations were all proved to be stable in the H structure and all exhibit semiconducting behavior, *i.e.*, MoO_2, MoS_2, $MoSe_2$ and $MoTe_2$.[22] For the OMoY monolayers in the present work, we calculated the formation energies (ESI†) and found that they are of the same order of magnitude as that of the MX_2 monolayers, suggesting that they have the same

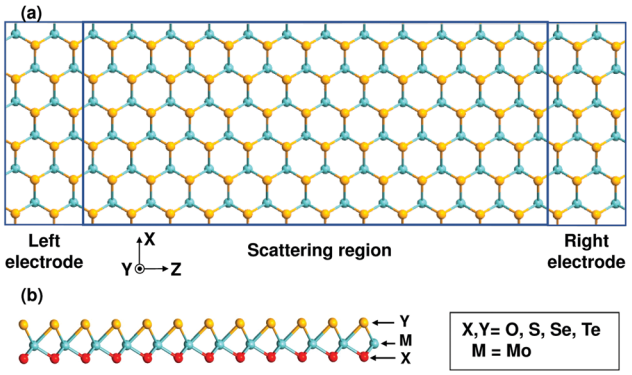

Fig. 1 (a) Top view of the Janus monolayer XMoY (X, Y = O, S, Se and Te). There are in total six kinds of XMoY structures, *i.e.*, OMoS, OMoSe, OMoTe, SMoSe, SMoTe and SeMoTe. (b) Side view of Janus OMoTe.

stability as the MX_2 ones.[22] For instance, the formation energy of the OMoTe monolayer is 2.13 eV, just between those of its parents (6.79 eV for MoO_2 and 0.89 eV for $MoTe_2$).[22] To explore the electronic transport properties, a two-probe configuration was constructed, consisting of the scattering region and left/right lead, as shown in Fig. 1(a). Before the transport calculations, all the two-faced configurations (including their cells) were fully optimized. As an example, Fig. 1 shows the geometry of the OMoTe monolayer. From the top view in Fig. 1(a), one finds that the hexagonal lattice is preserved. From the side view, one can clearly see that the structure is asymmetric in the out-of-plane direction, as shown in Fig. 1(b). Obviously, the bond length of Mo–S is larger than that of Mo–O.

Fig. 2 shows the transmission spectra of these Janus monolayers along the zigzag direction, which is the transport direction studied in this work, as shown in Fig. 1(a). One finds that there are five XMoY configurations exhibiting semiconductor behavior, *i.e.*, OMoS, OMoSe, SMoSe, SMoTe and SeMoTe. Around the Fermi level, there is a transmission gap for each case, whose width varies with the elemental combination. As their parent materials are all semiconductors, those are easily understood. However, Janus OMoTe exhibits metallic behavior, where the transmission is finite at the Fermi energy.

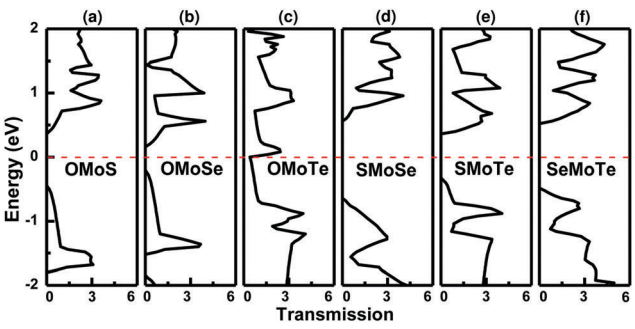

Fig. 2 (a–f) Transmission spectra of the Janus monolayers of OMoS, OMoSe, OMoTe, SMoSe, SMoTe and SeMoTe, respectively. In particular, the OMoTe monolayer exhibits metallic behaviour. Others exhibit semiconducting behavior. The Fermi energy was set to be zero.

This is quite different from the other cases. More interestingly, its parents (MoO_2 and $MoTe_2$) are both semiconductors.

In the present work, the parent and child materials possess the same geometry, *i.e.*, MX_2. Moreover, the M atoms in the middle layer are the same for the three materials (parents and the child), *i.e.*, Mo. Particularly, the X and Y atoms from the two parents that constitute the face layers of the child are in the same group in the periodic table, *i.e.*, chalcogen. That is to say, the X and Y atoms share the same electronic configuration in the outermost orbitals (here, X, Y = O, S, Se and Te). As is well known, elements in the same group tend to exhibit quite similar properties due to the same electronic configuration. Based on these factors, we roughly concluded that the child tends to possess the same properties as its parents, *e.g.* semiconducting. Such a conclusion is confirmed by almost all the child materials in the present work except OMoTe. So, for OMoTe, it is surprising and important that the two semiconducting ''parents'' produce a metallic ''child''.

To gain insight into the origin of these transport behaviors, we calculated the band structures of these monolayers, as shown in Fig. 3. One finds that in the band structure of OMoTe, there are two bands across the Fermi level. Apparently, it is these bands that contribute to the finite transmission for OMoTe. Moreover, in both Γ–X and Γ–Z k-point directions, there is a band across the E_F. So, in both of these two directions, the Janus OMoTe monolayer exhibits metallic behaviour. Above the Fermi level, there are another two bands. Although they do not cross the E_F, they intersect with the bands that cross the E_F. As a result, there is no band gap around the E_F. And, they consequently contribute to the continuous transmission in Fig. 2(c), where there is no transmission gap around the E_F.

For the other Janus monolayers, there is a band gap at the Fermi level for each case, see Fig. 3. Obviously, it is those band gaps that result in the transmission gaps in Fig. 2. Besides, like the OMoTe case, the band structures of those configurations show the same behavior between Γ–X and Γ–Z k-point directions, *i.e.*, they exhibit the semiconductor feature in both of these two directions. In brief, the metallic/semiconductor behavior is robust to the direction of the monolayer for both OMoTe and the other cases. Such robustness would be quite beneficial in the development of practical devices.

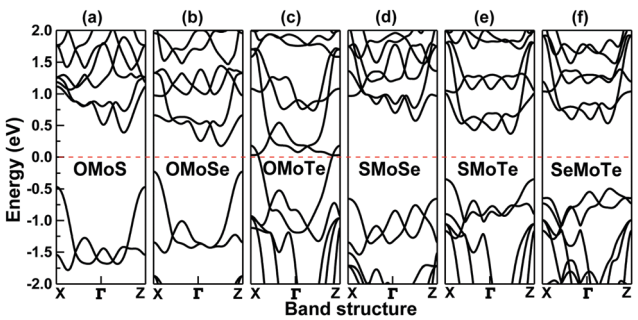

Fig. 3 (a)–(f) Band structures of the Janus monolayers of OMoS, OMoSe, OMoTe, SMoSe, SMoTe and SeMoTe, respectively. There are bands across the Fermi level for OMoTe.

We next investigated the underlying mechanism of the strange electronic behavior of OMoTe. Previous studies show that the band gap of MX_2 monolayers is very sensitive to applied strain, which is usually used as a modulating method for bandgap engineering.[27–33] For our OMoTe structure, the asymmetry between the top and bottom layers could naturally induce extra strain, which may be responsible for the semiconductor–metal transition. To prove this, we started with its parents and applied strain on them, *i.e.*, MoO_2 and $MoTe_2$. The lateral lattice parameters of the MoO_2 and $MoTe_2$ monolayers are a = 2.78 and 3.46 Å, respectively. And, the optimized lattice parameter of Janus OMoTe is a = 3.24 Å. Interestingly, when we force the lattice parameters of MoO_2 and $MoTe_2$ to be 3.24 Å, they both become metallic (ESI†). In other words, both of the parents become metallic when they share the lattice parameter of their ''child''. Note that these transitions occur without altering the elements; they are solely induced by the strain. This validates our assumption of the mechanism of the strain-induced semiconductor–metal transition. Moreover, the trends of the parameter changes are not the same, where that of MoO_2 increases (from 2.78 to 3.24 Å) and that of $MoTe_2$ decreases (from 3.46 to 3.24 Å). It is actually reasonable that the lattice parameter of the child is in the middle of that of its parents.

For the two-faced Janus OMoTe monolayer, its top/bottom layer is full of O/Te atoms. If the strain is the key to trigger the semiconductor–metal transition, changing the ratio between O and Te atoms should alter the strain. Here, we argue that the transition could be progressive if we carefully control the ratio of O to Te atoms. To demonstrate this, we set up a larger supercell where there are eight atoms in each layer (top/middle/bottom), as shown in Fig. 4(j). Starting with $MoTe_2$, we increased the ratio of O atoms in one layer. The structure can be denoted as $O_{n/8}MoTe_{2-n/8}$ with n varying from 0 to 8, where n = 0 stands for $MoTe_2$ and n = 8 stands for Janus OMoTe. Fig. 4(a)–(i) show the transmission spectra of all these cases with n = 0 to 8, respectively. In Fig. 4(a), one finds that there is a transmission gap around E_F, suggesting $MoTe_2$ is a semiconductor. When we substituted one O atom for one Te atom in the supercell, the transmission gap remains but its width decreases, as shown in Fig. 4(b). When there are two substituted O atoms, the configuration becomes the structure shown in Fig. 4(j), where n = 2. This time, the transmission gap becomes much smaller. When the ratio of substituting O atoms increases further from Fig. 4(c)–(g), one easily finds that the transmission gap decreases gradually. All of them (from Fig. 4(c)–(g)) are semiconductors.

Note that the gap in Fig. 4(g) (n = 6) has already become very small compared with that of Fig. 4(a). However, when there are seven substituted O atoms in the top layer, the situation changes quite a lot, see Fig. 4(h). The transmission gap disappears and there is a finite transmission at (and around) the E_F. Now, the monolayer becomes metallic. So, although there is still Te atoms in the top layer, the configuration has changed to become metallic. When the ratio of the O atoms further increases, the configuration becomes the two-faced Janus OMoTe. Naturally, the transmission around the E_F further increases, see Fig. 4(i).

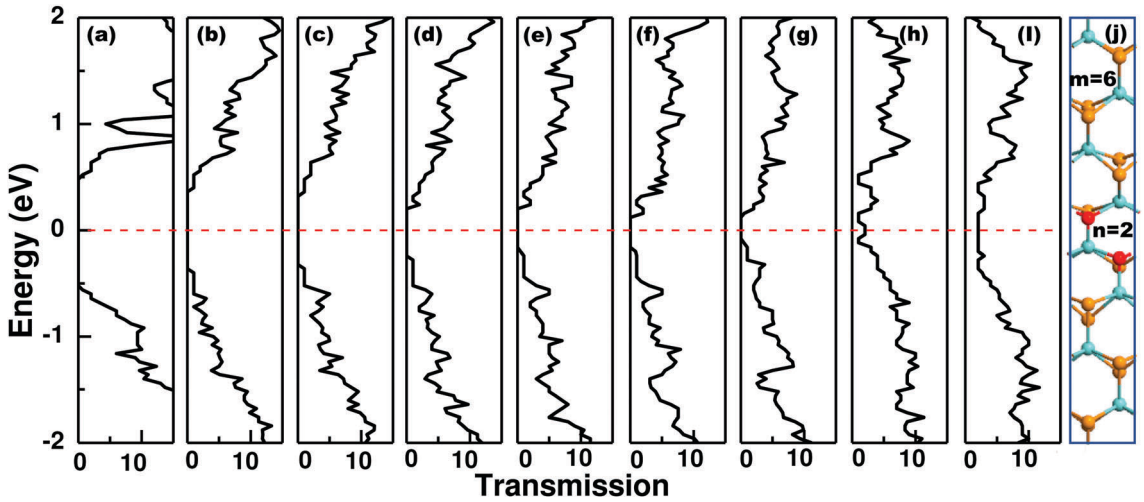

Fig. 4 (a–i) Transmission spectra of $O_{n/8}MoTe_{2-n/8}$ with n varying from 0 to 8, where we use an O atom to substitute Te in the top layer of the 2D structure. (j) Top view of the supercell of $O_{2/8}MoTe_{2-2/8}$ (shown as an example). The leftmost and rightmost bands correspond to $MoTe_2$ and OMoTe, respectively. Note that there are 8 pairs of Te atoms in the supercell of $MoTe_2$. From (a) to (i), the ratio of O atoms increases, but the transmission gap decreases. Each configuration has been optimized.

To trace the origin of the transmission, we also calculated the band structures of all the $O_{n/8}MoTe_{2-n/8}$ configurations. They are shown in Fig. 5(a)–(i), corresponding to the transmission spectra in Fig. 4(a)–(i), respectively. As we can see, from Fig. 5(a)–(i), the conduction band moves down gradually, whereas the valence band moves up gradually. And in Fig. 5(h), they both cross the Fermi level. As a result, the band gap decreases gradually and finally disappears from left to right in Fig. 5. So, it is those variations in the band structures that result in the change of the transmission spectra in Fig. 4. The process can be seen as a "progressive transition".

Limited by calculating resources, in the present work, we chose the supercell with only eight Mo atoms. According to the strain mechanism, a more gradual change of the band gap could be observed in larger supercells, where the ratio of O to Te atoms could be modulated more gradually (now the changing step is 1/8). During the change of band gap, there should be a critical state where the band gap is zero. With a larger supercell, this critical state will be easier to find. In this work, we confined our studies to the situation where the O atoms distribute in one face. In Fig. 4 and 5, the O atoms are adjacent with each other (all the corresponding structures are presented in the ESI†). Besides them, we constructed another 23 configurations with the same supercell and calculated the corresponding band structures and transmission spectra (ESI†). Considering the symmetry, all the possible configurations in this supercell have been studied. It was found that the bandgap (or transmission gap) decreases with an increase of the O content, and this is the main trend of the bandgap variation. The distribution of O atoms has only a slight influence on it. Importantly, the semiconductor–metal transition occurs at almost the same ratio of O atoms as the adjacent ones. So, the key factor is the ratio of O atoms, not their distribution (for the one-face condition). This would be quite beneficial for practical applications. Note that this conclusion is drawn for this supercell.

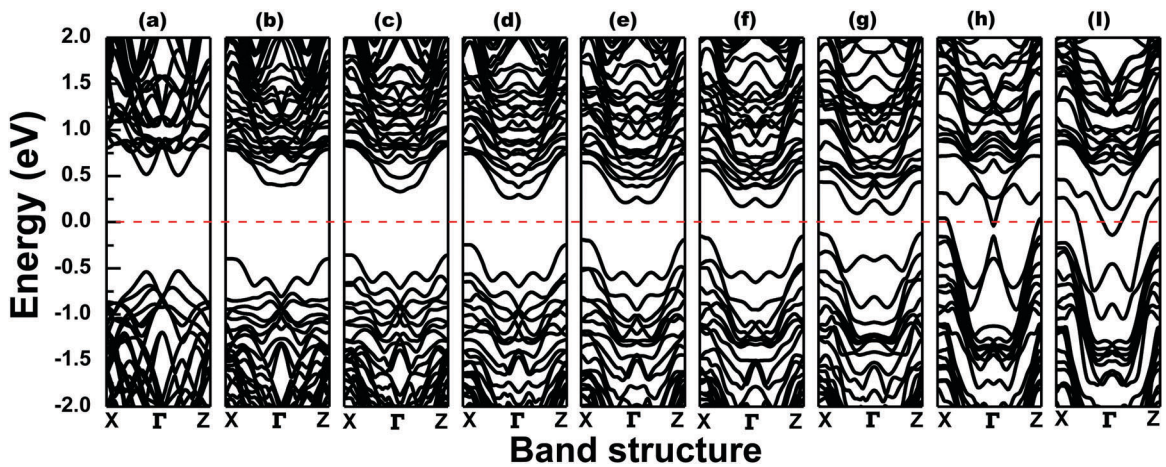

Fig. 5 (a–i) Band structures of $O_{n/8}MoTe_{2-n/8}$ with n varying from 0 to 8, corresponding to Fig. 4(a–i), respectively.

Further studies with larger supercells require systematic investigation and much more calculating resources, which we hope to do in the future.

It should be noted that in all the $O_{n/8}MoTe_{2-n/8}$ configurations, only $MoTe_2$ is a direct band gap semiconductor, the others are indirect ones. The Janus OMoTe is also an indirect one. That is to say, the introduction of O atoms changes $MoTe_2$ from a direct band gap semiconductor to an indirect one. This can actually be used as a way to modulate the electronic structure of the MX_2 monolayer. Note that not all the two-faced Janus monolayers are indirect band gap semiconductors. In Fig. 3, one finds that OMoS, OMoSe, SMoSe and SMoTe are indirect band gap semiconductors, but SeMoTe is a direct one.

During the geometry optimization, any residual force would be eliminated. In the present work, the ''strain'' is introduced to explain the metal–semiconductor transition. Although O and Te are in the same group in the periodic table, a substitution between them in MX_2 (without optimization) will no doubt induce extra strain, as they are in different periods and possess different atomic radii. If we assume that OMoTe is obtained by substituting the element in one of the parents, it is this ''strain'' that triggers the deformation of the new structure and results in the new properties. Of course, the strain will finally be released through the variations of the geometries during optimization (such as lattice parameter and bond length). We compared the lattice parameter of OMoTe and its parents and observed its difference and effect. In addition, we also calculated the bond lengths of OMoTe and its parents (ESI†). It was found that for the Mn–O or Mo–Te bond, it is different from that of the parents. According to the above proposed mechanism, this is caused by the release of strain. So, if we try to describe and rationalize the ''strain'', we could use the variations of the lattice parameter and bond length (or some other geometric parameters, such as bond angle).

In fact, a transition will happen suddenly, it will not be progressive. However, in our system, the bandgap (or transmission gap) decreases gradually with the increase of oxygen concentration and finally disappears, *i.e.*, it triggers the semiconductor–metal transition. Although the transition finally occurs when the ratio of O atoms increases to a specific value, it tends to occur even when that ratio is very small. So, ''progressive'' in the present work refers to the trend of the whole transition process (or the variation of the bandgap). In some way, the bandgap could be used as an index to distinguish between the semiconductor and metal. Moreover, we have found that the O distribution only has a very slight influence on the bandgap variation and transition, and the key factor is O ratio (ESI†). So, by modulating the O ratio, it would be easy to produce the transition in practice.

From the energetic point of view, it was found that the geometric form of the OMoTe nanotube is preferred, compared with planar structures (ESI†). Interestingly, the OMoTe nanotube becomes semiconducting. The underlying mechanisms are worth exploring, but they are out of the scope of the present work and will be studied in the future. Moreover, through optimization, we find that a nanoribbon cutting from the monolayer may not be able to roll up to a nanotube spontaneously, and it tends to keep the planar structure (ESI†).

Former studies showed that an external strain could effectively modulate the band gap of the MX_2 monolayer.[27–33] However, the obtained properties are not the intrinsic feature of the material. So, once the external stain is withdrawn, the monolayer would exhibit the original electronic properties, *i.e.*, the modulating effect cannot persist. On the other hand, for the Janus monolayer, its geometry is stable and the electronic features are its intrinsic ones, which can persist without the need of additional equipment. This could be quite beneficial for the fabrication of realistic devices.

As is well known, there are plenty of MX_2 monolayers.[22] That is to say, there are many candidate elements for M and X. So, the number of possible combinations of Janus XMY would be quite large. This provides us with a huge database to explore and select Janus XMY monolayers, which are expected to be used for building interesting practical nanoelectronic devices.

Conclusions

In summary, we studied the electronic structure and transport of Janus XMoY monolayers (X, Y = O, S, Se and Te) through first-principles calculations. It was found that the OMoTe monolayer exhibits metallic behavior, and the others are semiconductors. Interestingly, the ''parents'' of OMoTe (MoO_2 and $MoTe_2$) are both semiconductors. Further analysis shows that it is the out-of-plane asymmetry-induced strain that results in the metal–semiconductor transition between Janus OMoTe and its parents. By increasing the ratio of O atoms in one face of $MoTe_2$, a progressive decreasing trend of the bandgap, as well as the transition to metallic, was found. This could be used as an effective way to precisely control the bandgap. Different from other methods, it uses the intrinsic feature of the structure, without the need of additional equipment. Moreover, it is expected to be extended to many other transition-metal chalcogenides, showing great application potential.

Conflicts of interest

There are no conflicts to declare.

Acknowledgements

This work was supported by the National Natural Science Foundation of China (NSFC11504178, NSFC11705097 and NSFC11774179), the Natural Science Foundation of Jiangsu Province (BK20150825, BK20170895, and BK20161513), the Scientific Research Foundation of Nanjing University of Posts and Telecommunications (NY217013, NY214151, NY217166 and NY215027), and the Natural Science Fund for Colleges and Universities in Jiangsu Province (17KJB140015, RK033STP16002 and 2016-JNHB-060).

References

1 K. S. Novoselov, A. K. Geim, S. V. Morozov, D. Jiang, Y. Zhang, S. V. Dubonos, I. V. Grigorieva and A. A. Firsov, *Science*, 2004, **306**, 666.
2 K. S. Novoselov, D. Jiang, F. Schedin, T. J. Booth, V. V. Khotkevich, S. V. Morozov and A. K. Geim, *Proc. Natl. Acad. Sci. U. S. A.*, 2005, **102**, 10451–10453.
3 A. Kis, *Nat. Nanotechnol.*, 2012, **7**, 683.
4 Z. Zeng, Z. Yin, X. Huang, H. Li, Q. He, G. Lu, F. Boey and H. Zhang, *Angew. Chem.*, 2011, **50**, 11093.
5 H. Schmidt, F. Giustiniano and G. Eda, *Chem. Soc. Rev.*, 2015, **46**, 7715–7736.
6 C. Tan and H. Zhang, *Chem. Soc. Rev.*, 2015, **44**, 2713–2731.
7 J. Zhang, S. Jia, I. Kholmanov, L. Dong, D. Er, W. Chen, H. Guo, Z. Jin, V. B. Shenoy and L. Shi, *ACS Nano*, 2017, **11**, 8192–8198.
8 S. Mao, J. Chang, H. Pu, G. Lu, Q. He, H. Zhang and J. Chen, *Chem. Soc. Rev.*, 2017, **46**, 6872–6904.
9 H. O. Churchill and P. Jarilloherrero, *Nat. Nanotechnol.*, 2014, **9**, 330.
10 S. Bhattacharyya and A. K. Singh, *Phys. Rev. B: Condens. Matter Mater. Phys.*, 2012, **86**, 075454.
11 A. C. Neto, F. Guinea, N. M. Peres, K. S. Novoselov and A. K. Geim, *Rev. Mod. Phys.*, 2009, **81**, 109.
12 A. K. Geim, *Science*, 2009, **324**, 1530–1534.
13 D. Haberer, D. Vyalikh, S. Taioli, B. Dora, M. Farjam, J. Fink, D. Marchenko, T. Pichler, K. Ziegler and S. Simonucci, *et al.*, *Nano Lett.*, 2010, **10**, 3360–3366.
14 A. Nikitin, L.-Å. Näslund, Z. Zhang and A. Nilsson, *Surf. Sci.*, 2008, **602**, 2575–2580.
15 Q. H. Wang, K. Kalantar-Zadeh, A. Kis, J. N. Coleman and M. S. Strano, *Nat. Nanotechnol.*, 2012, **7**, 699.
16 K. F. Mak, C. Lee, J. Hone, J. Shan and T. F. Heinz, *Phys. Rev. Lett.*, 2010, **105**, 136805.
17 M. Chhowalla, H. S. Shin, G. Eda, L. J. Li, K. P. Loh and H. Zhang, *Nat. Chem.*, 2013, **5**, 263–275.
18 B. Radisavljevic and A. Kis, *Nat. Mater.*, 2013, **12**, 815.
19 Y. Gong, J. Lin, X. Wang, G. Shi, S. Lei, Z. Lin, X. Zou, G. Ye, R. Vajtai and B. I. Yakobson, *et al.*, *Nat. Mater.*, 2014, **13**, 1135.
20 M.-Y. Li, Y. Shi, C.-C. Cheng, L.-S. Lu, Y.-C. Lin, H.-L. Tang, M.-L. Tsai, C.-W. Chu, K.-H. Wei and J.-H. He, *et al.*, *Science*, 2015, **349**, 524–528.
21 Y. Gong, S. Lei, G. Ye, B. Li, Y. He, K. Keyshar, X. Zhang, Q. Wang, J. Lou and Z. Liu, *et al.*, *Nano Lett.*, 2015, **15**, 6135–6141.
22 C. Ataca, H. Sahin and S. Ciraci, *J. Phys. Chem. C*, 2012, **116**, 8983.
23 M. Brandbyge, J.-L. Mozos, P. Ordejón, J. Taylor and K. Stokbro, *Phys. Rev. B: Condens. Matter Mater. Phys.*, 2002, **65**, 165401.
24 J. Taylor, H. Guo and J. Wang, *Phys. Rev. B: Condens. Matter Mater. Phys.*, 2001, **63**, 245407.
25 H. J. Monkhorst and J. D. Pack, *Phys. Rev. B: Solid State*, 1976, **13**, 5188–5192.
26 J. P. Perdew, K. Burke and M. Ernzerhof, *Phys. Rev. Lett.*, 1996, **77**, 3865–3868.
27 J. R. Brent, N. Savjani and P. O'Brien, *Prog. Mater. Sci.*, 2017, **89**, 411–478.
28 G. G. Naumis, S. Barraza-Lopez, M. Oliva-Leyva and H. Terrones, *Rep. Prog. Phys.*, 2017, **80**, 096501.
29 S. B. Desai, G. Seol, J. S. Kang, H. Fang, C. Battaglia, R. Kapadia, J. W. Ager, J. Guo and A. Javey, *Nano Lett.*, 2014, **14**, 4592–4597.
30 C.-H. Chang, X. Fan, S.-H. Lin and J.-L. Kuo, *Phys. Rev. B: Condens. Matter Mater. Phys.*, 2013, **88**, 195420.
31 M. Ghorbani-Asl, S. Borini, A. Kuc and T. Heine, *Phys. Rev. B: Condens. Matter Mater. Phys.*, 2013, **87**, 235434.
32 H. Pan and Y.-W. Zhang, *J. Phys. Chem. C*, 2012, **116**, 11752–11757.
33 H. Peelaers and C. G. Van de Walle, *Phys. Rev. B: Condens. Matter Mater. Phys.*, 2012, **86**, 241401.